Report on Neutron Detectors for G_E^n

A. Lewandowski
University of Virginia

August 28, 1997

Abstract

To understand and test the operation of large volume neutron detectors the behavior of scintillated light produced from cosmic ray muons in these detectors was observed. The pulse height as a function of position was measured as was an effective velocity within the material. Position and time resolutions within the bar were also determined. The observed effects were dependent on the detector and light pipe geometries.

1 Introduction

To measure quasielastic scattering of an electron from a neutron it is necessary to detect the recoil neutron in some fashion. Large volume scintillation detectors were created for this purpose in an experiment to measure the charge form factor of the neutron.

A high energy neutron is a very penetrating particle interacting predominantly with the nuclei of the interaction medium. The principle energy loss mechanism for high energy neutrons is elastic scattering. When they interact with particles in a scintillating material they produces charged particles largely by the (n,p) scattering process [1]. The protons in turn produce light in the scintillator which can be detected. To understand the detection of neutrons it is necessary, therefore, to understand the behavior of light within the bar detectors. This paper largely describes the measurements taken to determine how scintillated light interacts within the neutron detectors.

Cosmic rays can be used to produce such light. Rays that pass completely through a material lose energy by ionization. The mean energy loss per g-cm^{-2} is given by the *Bethe-Bloch formula*,

$$-\frac{dE}{dx} = \frac{NZ}{A}\frac{2\pi Z'^2 e^4}{mv^2}[\ln\frac{2mv^2W\gamma^2}{I^2(Z)} - \beta^2]$$

in an interaction medium consisting of atoms of atomic number Z, mass number A, and average ionization potential $I(Z)$. The incident particle has charge $Z'e$

and velocity v with $\beta = v/c$ and $\gamma = (1 - \beta^2)^{-1/2}$. The mean energy loss is then dependent on the initial energy of the cosmic but predominantly on the distance traveled in the medium. For air the minimum mean energy loss by ionization can be taken to be 2 MeV per g-cm^{-2}. [2].

When a charged particle interacts within a plastic scintillator such as the cosmic ray muons used in this experiment, delocalized electrons in π-molecular orbitals are excited into higher energy states. These states decay to the lowest excited singlet state. When the electron decays from this state, denoted S*, light is emitted. The decaying electron falls not to the ground state, however, but to an excited vibrational level of the ground state. The energy of the emitted light, then, is not sufficient to excite other electrons in the scintillator and so may travel through. The plastic scintillator produces an extremely fast signal from this reaction. The signal can be described mathematically by the formula,

$$N(t) = N_0 f(\sigma, t) \exp(\frac{-t}{\tau})$$

where $f(\sigma, t)$ is a Gaussian with standard deviation σ.

Light emitted by the scintillator may be absorbed by the walls of the scintillator or in the material itself. Light loss occurs predominantly through loss in the walls when the angle of the light is less than the critical angle, $\theta_c = \arcsin \frac{n_{out}}{n_{scint}}$. Any ray hitting the side of the bar at an angle greater than this angle will be completely reflected. The amount of light loss can be described mathematically by the following equation giving intensity as a function of distance:

$$L(x) = L_0 \exp(\frac{-x}{l}) \quad (1)$$

Here, L_0 is the incident intensity of the light and l is the attenuation length.

We wish to measure the attenuation along the length of the bar as seen by the photomultiplier tubes at each end. In addition we wish to measure the effective velocity of light in the material. These measurements will also provide an expected time and position resolution for these detectors. With this information it should be possible to determine the position of an interaction anywhere in the bar within the determined resolution.

2 Apparatus and Procedure

The neutron detectors used in this experiment are composed of a scintillating bar made from BC408 plastic. The bar dimensions are 10 cm x 10 cm x 160 cm. Attached to the ends of the bar are light pipes approximately 9 cm long. These light pipes converge to the face of the Phillips XP2262 photomultiplier tubes (PMTs) attached at each end.

Cosmic ray muons were used as the incident particles. To localize the cosmics within a certain area of the bar two trigger paddles were used. These paddles

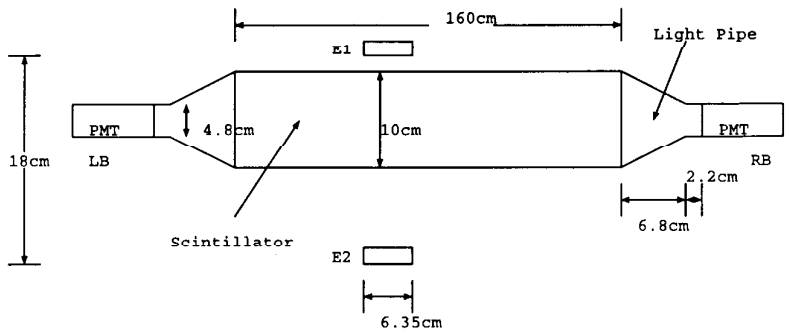

Figure 1: The bar and paddle configuration and dimensions

consist of a scintillating plastic (6.35 cm x 17.8 cm x 0.9 cm) attached to a PMT by a light pipe. The configuration of these paddles in relation to the bar detector and the dimensions can be seen in figure 1.

A diagram of the circuit used in this experiment is displayed in figure 2. The two photomultiplier tubes are distinguished as left bar (LB) and right bar (RB). The two paddle counters are referred to as ΔE1 and ΔE2 where they refer to the top and bottom paddles respectively. Two analog-to-digital converters are used in this experiment: the LeCroy 2249A ADC and the LeCroy 4300B Fast Encoding and Readout (FERA) ADC. I will refer to the second as the FERA and specify the first whenever necessary. Both are 10 bit, charge integrating with a 256 pC range. Two time-to-digital converters were also used in this experiment: the LeCroy 2228A TDC and the LeCroy 4303 Time-to-FERA Converter in conjunction with a LeCroy 4300B FERA ADC. The second will be referred to as the TFC. Additional circuit elements are listed in table 1.

High voltage to the PMTs is set such that the output signal can be viewed within the range of the analog to digital converters. The linear signal from each PMT is passed through a discrimator with the threshold voltage set such that much of the noise is removed from the circuit. The LB signal is used to start a time-to-digital converter while the RB signal stops it. This information can be used to obtain a quick view of the time difference within the bar. The two Δ counters form a coincidence which signals a cosmic ray passing through the bar. An OR is made with the LB and RB signals and this signal is used to trigger the start of the ADC and FERA gates in coincidence with the Δ coincidence. The Δ coincidence is further used in coincidence with the ORed bar signal to start the TFC. This TFC is stopped individually by the discriminated output from LB, RB and the ΔE coincidence.

The circuit was set up with a pulser operating at 10.4 kHz and 920 mV with

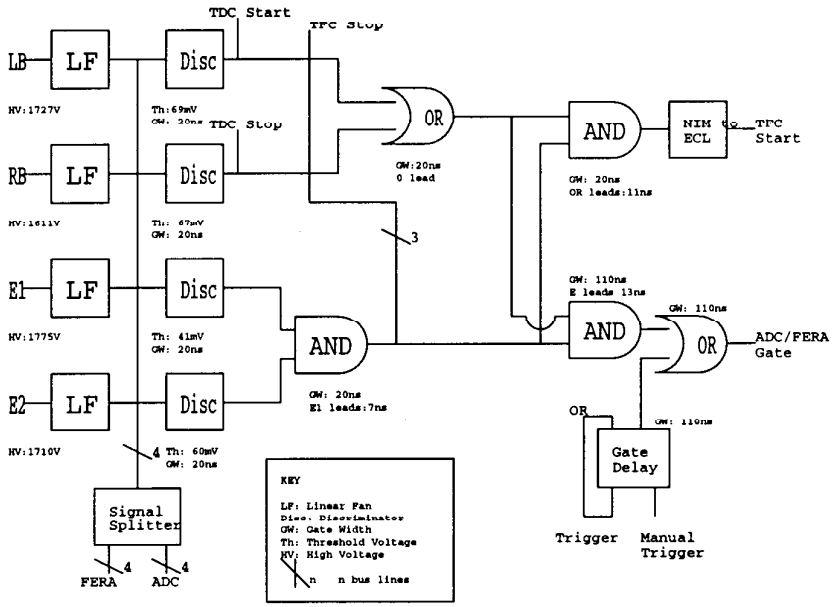

Figure 2: Circuit Diagram

Make	Model	Function
PS	740	Quad Linear Fan-In/Out
LeCroy	4608C	Octal Discriminator
LeCroy	622	Quad Coincidence
Tennelec	TC 412A	Delay
UVA	122B	Signal Splitter
LeCroy	4616	ECL-NIM-ECL
LeCroy	429A	Logic Fan-In/Out
LeCroy	HV4032A	High Voltage Power System
PS	700	NIM Crate
LeCroy	8901A	GPIB Interface
LeCroy	1434A	Camac Crate
PS	794	Quad Gate Delay/Generator
PS	417	NIM Pocket Pulser

Table 1: Electronic equipment

a FWHM of 6 ns. The pulsed signal was sent through a fifth linear fan to each of the fan inputs. All timing and gate width measurements were taken with the pulser. The pulser was used in conjunction with the delay box to calibrate the TFC. By adding delay in 2 ns intervals one can quickly generate a histogram of these intervals. By measuring the peak locations it is possible to measure the channel resolution. For this circuit the TFC signal stopped with the left had 52.9 ps/channel while that for the right had 51.9 ps/channel. The standard deviation of the peaks generated by the pulser correspond to 88 ps on the TFC. The discriminator thresholds were adjusted with the PMT signals.

The basic reasoning of the circuit is this: The 2249A ADC and the FERA measure the energy spectrum of cosmics passing through an area of the bar specified by the Δs. By moving the paddles the energy spectrum seen by these devices shifts. From the peak energy at various points along the bar a plot of energy versus distance from a PMT can be constructed. From this data a measured attenuation length can be calculated. In addition, the TFC measures the time it takes a light signal to reach the ends of the bar once it has been received at the Δs. That time increases or decreases as the paddles are moved towards or away from a PMT. From this timing information one can construct a plot of time versus distance from which the effective velocity of light in the material can be determined.

3 FERA Results and Analysis

The primary data was taken after runs of 5000 cosmic ray hits. A hit is an event where a cosmic ray passes through both ΔE paddles and triggers an event in the bar. With the circuit described above it takes about six hours and 15 minutes to generate that many counts. Ten 5000 count runs were taken at 15.24 cm (6 in) intervals along the bar. Data was stored in a ROOT tree structure using the program, `treegen.C`. The source code for that program can be found at the end of this paper. (ROOT is a new data handling program from CERN and is used throughout this experiment. A brief summary of ROOT operation and capability is contained in appendix A.)

Sample FERA output is contained in figure 3. This output takes the shown form due to zenith angle spread of the cosmics in the atmosphere as well as the energy spread of the incident cosmics. Statistical fluctuations in the energy loss account for most of the width of the peak, however. The tail arises from large single collision energy transfers as well as energy loss from bremsstrahlung. This is described mathematically by the theory of Landau for thin absorbers. Assuming the mean energy deposited in the bar to be similar to that in air (2 MeV/g-cm^{-2}) the energy peak represents a deposited energy of about 20 MeV. This output was fit with the sum of two Gaussians,

$$p_1 \exp(-\frac{(x-p_2)^2}{2p_3^2}) + p_4 \exp(-\frac{(x-p_5)^2}{2p_6^2})$$

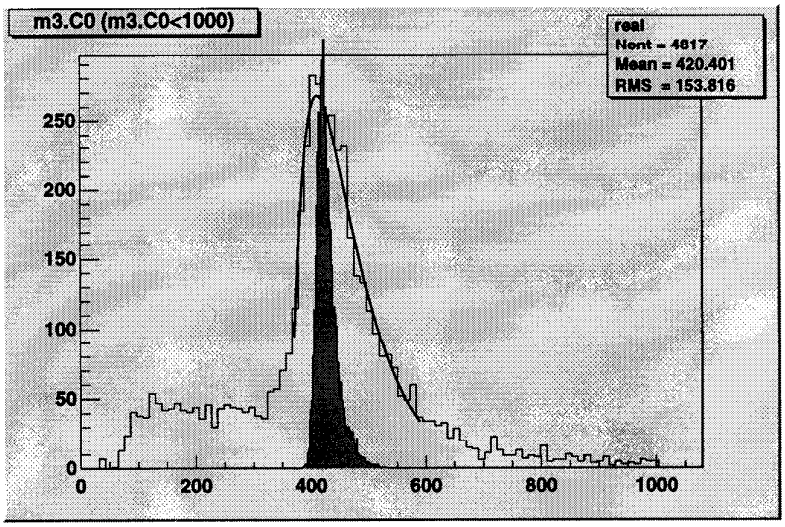

Figure 3: Sample FERA data with Gauss+Gauss fit. The darker plot in the foreground is from a Monte Carlo simulation

where p_1, $p_2 \ldots p_6$ are parameters to be fit with the data. The fitting routine used was that supplied by the ROOT program. The fitted parameters describe a function whose maximum can be found numerically. The results are contained in table 2 and a plot of the data is contained in figure 4.

As stated in the introduction one expects an exponential attenuation along the bar as given by equation 1. The data, however, does not conform well to such a fit. An attenuation length across 137 cm of the bar was calculated and found to be 358 cm for the RB signal and 634 cm for the LB signal. A fit with an exponential and a reflective term,

$$L(x) = a(\exp(-\frac{x}{l}) + \exp(-\frac{320 - x}{l}) \tag{2}$$

was much nicer than the simple exponential. Here a and l are parameters to be fit with the data. Parameter, l, will be referred to as the attenuation length in place of the parameter, l, of equation 1. The attenuation lengths, then, found from these fits were 168 cm and 222 cm for the RB and LB signals respectively.

For an accurate understanding of the data it is necessary to take into account the contributions to the energy signal from reflections. To first order the energy deposited by the cosmic in the bar travels directly from its location in the bar to the PMT in the form of light. If this were the only observed effect the data

x (cm) from right	RB peak	LB peak	x (cm) from left
9.5	536.9	369.4	150.5
24.8	480	371.3	135.2
40.0	445.8	373.5	120.0
55.2	437.3	385.0	104.8
70.5	410.4	381.3	89.5
85.7	397.6	396.6	74.3
101.0	387.7	410.7	59.0
116.2	370.7	417.2	43.8
131.4	370.9	440.0	28.6
146.7	366.1	458.7	13.3

Table 2: FERA peak height measurements along the detector

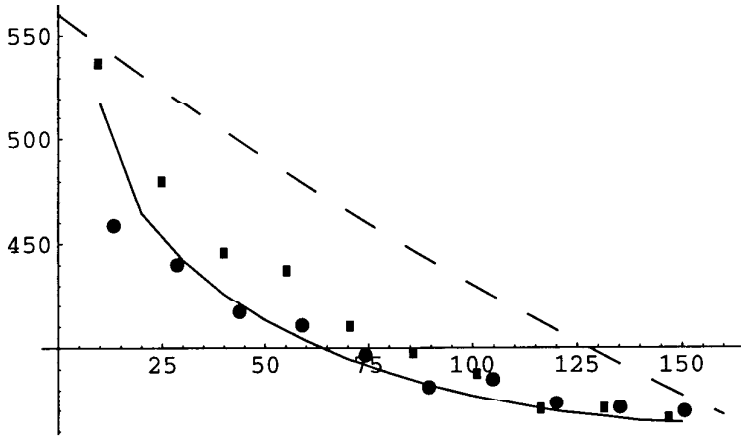

Figure 4: FERA pulse height vs. distance. Square points are RB peaks and circles are LB peaks. Pulse heights are given in channels with 0.25 pC/channel. The solid line is data taken from a Monte Carlo simulation. The dashed line is an exponential plot with the manufacturer specified attenuation length (3.8 m).

would fit an exponential curve given by equation 1. However, light created by the cosmic may also travel in the reverse direction, away from the PMT, reflecting off the PMT at the opposite end of the bar and later forming a signal in the first PMT. In addition, light emitted at some angle with respect to the bar will reflect along the sides of the bar traversing a longer distance and therefore becoming increasingly attenuated. A proper model of this interaction will incorporate all angles of travel for the light beam.

The darker histogram in the foreground in figure 3 is output from a Monte Carlo code simulating the interaction of light in the bar. When cosmic rays enter the atmosphere they are influenced by the earth's magnetic field causing distributional asymmetries known as the latitude effect and the east-west effect [3]. To first order, however, these asymmetries can be neglected and a $\cos^2\theta$ distribution assumed where θ is the angle with respect to the vertical [4]. Rays with this distribution were passed through an area defined by the paddles as in the true experiment. Energy produced was proportional to the distance the ray traveled in the bar. Light was emitted from a point centered in the bar (not along the length, of course) in all directions uniform in solid angle. Half the light was reflected off the light pipe surfaces (both left and right). Any rays hitting the side of the bar at an angle greater than the critical angle were discarded (assuming an index of refraction of 1.5). Any ray hitting the light pipe and not reflected was assumed to reach the PMT with no reduction in intensity.

Output from this code was obtained for 15 points along the bar. As seen in figure 3 the output is considerably more narrow than the data. This results from zero statistical fluctuations in energy loss. The slight tail at the upper end of the distribution is not a model of the Landau tail of the true data but is a result of the cosmic ray distribution. Additional reasons for the relative narrowness are lack of noise and zero energy spread of the incident cosmics. Like the true data, the Monte Carlo data does not conform well to the simple exponential of equation 1. Across 140 cm of the bar we arrive at an attenuation length of 399 cm. Using the fit of equation 2, an attenuation length of 181 cm was calculated. We see then from this simple model that large shifts in light loss are possible including only geometrical considerations. The plot of pulse height versus distance from this code is shown as the solid line in figure 4. As seen it conforms fairly well to the measured plots. Adding light pipe geometry and second order reflections to the model would further improve the results. Because of the large effect reflections have on the pulse height, it is thought that discrepancies in reflectivity may account for at least some of the difference in attenuation length between the RB and LB signals. This is supported by work done by R. Madey et al. [5]. A copy of the source code for this Monte Carlo, denoted `tfcprog.C`, can be found at the end of this paper.

One can arrive at a qualitative understanding of the particular bar measured by examining figure 4. One will notice that both the Monte Carlo and the RB signals rise fairly rapidly under 25 cm but the LB signal does not. This can be explained by a high reflectivity at the LB end of light emitted near that end.

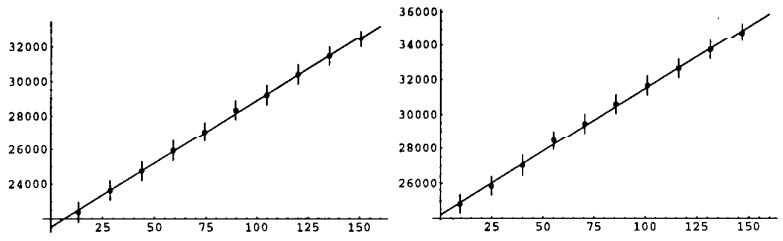

Figure 5: TFC peak values (ps) vs. distance (cm) (LB at left, RB at right)

These reflections become less pronounced at greater distance where the light pipes which cause the reflections have a lesser effect. Because the reflectivity in the model was assumed to be 50% we can say that the LB reflectivity for near sources is greater than that while reflectivity of the right for near sources is slightly less than that amount.

4 TFC Results and Analysis

TFC output is Gaussian distributed. Gaussian fits were applied to this data for the LB and RB signals and the peak values recorded. A plot of these values versus distance is contained in figure 5.

A similar situation as that for the FERA data occurs for the TFC with an additional complication. The TFC is started with the Δ coincidence. The signal stopped with the Δ coincidence is, therefore, well defined. The signals stopped by the LB and RB signals are subject to fluctuations due to geometric, resolution, and walk factors.

TFC walk arises from varying rise times of PMT output pulses. According to Leo the output voltage of a PMT is given by,

$$V(t) = -\frac{GNeR}{\tau - \tau_s}[\exp(-\frac{t}{\tau_s}) - exp(-\frac{t}{\tau})]$$

for $\tau \neq \tau_s$ where τ = RC, G is the PM gain; N the number of photoelectrons emitted by the cathode; e the charge of the electron; τ_s the decay constant of the scintillator [1]. This equation describes an inverse pulse widening and increasing in magnitude as the gain is increased. It peaks at a particular time for all gain at a constant τ. Because the threshold voltage of a discriminator is constant, it outputs a gate whenever the input voltage passes a certain height. Because small PMT signals rise slower than large ones according to the above equation, small signals cause a TFC stop later than the large ones. For the small number of data points in this experiment the above equation can be approximated with

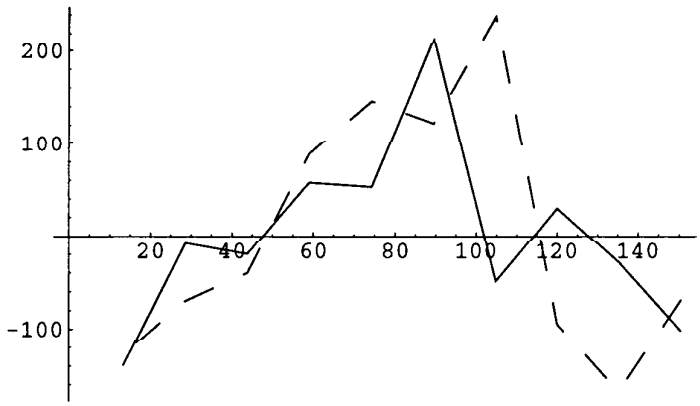

Figure 6: Residual plot from fitted line for TFC data. The dotted and solid lines are the RB and LB signals respectively. Distance along the horizontal axis is cm from the left. The vertical scale is in ps.

a parabola at the threshold voltage. Using this fit one can arrive at the following walk correction equation,

$$\Delta t = G(\frac{1}{\sqrt{ADC}} - \frac{1}{\sqrt{ADC_0}}) \tag{3}$$

where ADC is the value of the ADC at some particular event, ADC_0 is the most likely value of the ADC at some position taken from table 2 and G is a gain term to be fitted to the data [6]. This walk correction equation was applied to the data before the peak measurements above were taken. The source code implementing this fix is contained in the file `walkfix.C` at the end of this paper.

Figure 5 contains the TFC data with a least square fit. The fits give an effective velocity of light in the bars of $1.36 \pm 0.31 \times 10^8$m/s for the LB data and $1.37 \pm 0.30 \times 10^8$m/s for the RB data. Due to the geometrical factors and reflections the effective speed of light is not constant throughout the bar. In fact, the index of refraction of the bar is approximately 1.5 giving a speed of light in the bar of 2.0×10^8m/s. This is clearly not the measured value. The speed of light in the bar as a function of distance should be faster at the ends of the bar due to the larger solid angle of a direct photon transfer. From the residual plot of figure 6 it is observed that for both LB and RB signals the residual is negative at the ends. A negative residual, in this case, corresponds to a faster velocity which is as one would expect. The residuals more or less rise and fall along the same path suggesting, again, the effect of geometrical factors.

According to experiments and computer simulations performed by R. Madey

et al. the size and length of the light pipe is very influential on the measured time dispersion [5]. They concluded that an optimum detector geometry has a light pipe length which is slightly longer than half the length of the scintillating material. The light pipes used in this experiment are substantially shorter than that ideal length and so a larger fraction of reflected light is expected. The decreased velocity of light within the material as well as the shifts in attenuation can be attributed to a large extent to the geometry and size of the light pipes.

The standard deviation from a Gaussian fit for TFC data was found to be 551.4 ±16.9 ps for the right and 576.6 ±23.2 ps for the left. This observed width is influenced by time resolution in the bar as well as time resolution in the Δs. To eliminate the effect of the Δs one may subtract the two signals thereby subtracting the Δ contribution. This gives a mean resolution of 327.3 ±13.6 ps. The Monte Carlo code used to measure pulse height variation, `tfcprog.C`, was also used to generate TFC data. It gave a TFC resolution of 175 ps. The code for the TFC included geometrical factors, zenith angle spread of the cosmics and circuit resolution. It did not include the time resolution of the PMTs.

One may use this same data to measure a position resolution in the bar. According to R. Madey et al. the position of an event in the scintillator is given by,

$$y = \frac{1}{2}(t_L - t_R)$$

By taking the mean time resolution calculated above and knowing the effective velocity in the bar one can calculate the position resolution. This is found to be 4.45 ±1.03 cm for the LB and 4.48 ±1.00 cm for the RB.

5 Conclusion

Measurements of the light interactions within the neutron detectors were taken. Pulse height measurements were found to vary considerably as a function of distance. The geometry of the scintillating blocks and the geometry of the light pipes affect the pulse height dramatically. Using equation 2 exponential fits give 168 cm and 222 cm for RB and LB signals. The large difference is attributed to differences in reflectivity at each end of the bar. The ends of this bar are roughly 50% reflective with the left being slightly more than that and the right being slightly less.

The effective speed of light in the scintillator was found to be equal within error for both signals. The speed was found to be greater near the ends of the bar. This is attributed to light pipe and bar geometry. A time resolution < 400 ps was obtained. A corresponding position resolution < 6 cm was also found.

This is not the ideal circuit setup and there are certainly methods to improve the data. Firstly, the second TDC in this circuit is largely useless because the signal is not formed in coincidence with the Δ counters. The signal is then completely independent of position and cosmics all along the bar are recorded.

If the Δ signal were placed in coincidence with the LB start signal to the TDC, data taken from this TDC could be used in conjunction with data from the TFC to increase the time resolution. A second way to improve the data would be to decrease the size of the Δ paddles and increase the vertical spacing between them. As was seen above, paddle width and spacing account for a large part of the time resolution. Of course, such an improvement would come at the cost of time and so might not be practical. Finally, for the ten runs described here the TFC resolution was roughly 52 ps/channel. The limiting resolution of the TFC is 50 ps/channel. It may be a good idea decrease the resolution to avoid nonlinearities which can occur at the limit.

I thank Joe Mitchell for his help in designing the experiment and analyzing the data. Without his help and instruction this experiment would not have taken place.

A A Note on ROOT

Throughout this experiment the CERN program ROOT has been employed. Because this program has been out for only a short time I will give a brief discussion of its capabilities. A complete discussion can be found in the *ROOT, Overview* or at *http://root.cern.ch* [7].

ROOT is a data analysis program released by CERN to handle large amounts of data in place of such programs as PAW and PIAF. The command language, macro and programming language are all in C++. This allows for the benefits of dynamic memory as well as the simplification provided by object oriented design. All root objects inherit from the common base class TObject. Classes include tree and ntuple classes, multidimensional histogramming classes, graphics classes, and many others.

For data storage ROOT replaces the Ntuple form from PAW with the object oriented tree structure. Here data is stored in a "tree" object which may have many "branches". These "branches" may have one or more "leaves" which contain the data. In the process of filling the tree a branch may become full in which case the leaves are placed in a "basket". ROOT also provides a range of collection classes for storing and organizing incoming data. All of the mentioned storage parts are created through object-oriented design and so can be accessed with simple member functions.

ROOT has the ability to create one, two or three dimensional histograms. Histograms may be manipulated in many ways once created. Fitting routines are supplied by the program. An excellent graphics library allows one to edit freely and create almost any graphics object.

ROOT employs a C++ command interface so accessing root objects can be done simply. Groups of commands can be stored in a file or macro which is run without compilation. This allows for rapid program production. Programs

using ROOT code can also be compiled with a standard C++ compiler if speed in operation is a requirement.

A few examples of ROOT programs are contained at the end of this report. The programs `treegen.C` and `walkfix.C` are ROOT macros created for this experiment. The program `Tmcfields.C` is a compilable ROOT program employed in the Monte Carlo routine described in the following section.

B Magnetic Field Monte Carlo

A Monte Carlo simulation of electrons scattering from a point in the magnetic field of the polarized target was created. These electrons are tracked to the slit of the High Momentum Spectrometer (HMS) in Hall C. Although not a part of the neutron detector experiment it is a part of G_E^n and has been part of my summer project. A discussion is included here for completeness.

The Monte Carlo program consists of three files: `Tmcfields.C`, `track.C` and `ran3.C`. The last file is simply a random number generator and is a C++ version of the code found in *Numerical Recipes in C* [8]. The header file linking the three programs is `track.h`. This program was compiled to run on Linux. The makefile used for compilation is also included at the end of this paper.

The file `track.C` consists of a function which takes as its inputs initial position and momenta for an electron. These parameters are passed by reference. The program tracks these particles through the field using a Runge-Kutta integration. The electron moves in the field according to the equation $m\vec{p}' = -e(\vec{\eta} \times \vec{B})$ where $\vec{\eta}$ is the proper velocity of the electron. The field at a particular point is found from a bilinear interpolation of the field around that point.

The file `Tmcfields.C` performs the Monte Carlo integration and contains the main driving routine. The program asks for a central momentum vector and spectrometer angle. When running the program one should decide where the spectrometer is to be placed before a run is taken. The program then calls the function in the file `track.C` at momenta and angles distributed uniformly in solid angle and uniformly in momenta within 10% of the central momentum. If a tracked particle will enter the HMS slit after traveling the necessary distance (129.4 cm) the particle's initial information is recorded. This process occurs for as many counts as the user specifies. The results are stored in a ROOT tree structure with a single branch with five leaves.

The results from four runs of this program are contained in table 3. Here θ_c is the angle of the central trajectory from the z-axis in the y,z plane of the B-field and P_c is the magnitude of that momentum. The bend angle is the angle between the initial momentum and the momentum when it leaves the B-field. The angles θ_{spec} and ϕ_{spec} specify the position of the spectrometer in relation to the B-field. Angle θ_{spec} is the rotation in the y,z plane of the field. Angle ϕ_{spec} is the subsequent rotation in the x, z plane. The angles have been chosen

Q^2 $(GeV/c)^2$	P_c GeV/c	θ_c	bend angle	θ_{spec}, ϕ_{spec}	$\Delta\Omega$ msr
0.50	2.583	12.95	1.04	12.89, 1.01	6.69
1.00	3.437	20.03	1.22	19.98, 1.19	6.58
1.50	3.171	22.66	1.50	22.59, 1.46	6.60
2.00	2.905	24.05	1.74	23.96, 1.69	6.66

Table 3: Monte Carlo results for 10,000 hits

so that the central momentum beam passes through the center of the HMS slit. The solid angle seen by the particles is the ratio of hits over tries multiplied by the solid angle over which particles were thrown. With no field present the spectrometer solid angle is 6.65 msr.

References

[1] W.R. Leo, *Techniques for Nuclear and Particle Physics Experiments.* Springer-Verlag, New York. (1987) (50-63,151-54,156,181-82).

[2] S. Hayakawa, *Cosmic Ray Physics.* John Wiley & Sons, New York. (1969) (1-53,75-80).

[3] B. Rossi *Cosmic Rays.* McGraw-Hill Book Company. New York. (1964) 173.

[4] L. Janossy. *Cosmic Rays.* Clarendon Press. Oxford. (1950) 5.

[5] R. Madey, J.W. Watson, M. Ahmad, B.D. Anderson, A.R. Baldwin, A.L. Casson, W. Casson, R.A Cecil, A. Fazely, J.M Knudson, C. Lebo, W. Pairsuwan, P.J Pella, J.C. Varga and T.R. Witten, *Nucl. Instr. and Meth.* 214 (1983) 401-413.

[6] D. Mack *Instructional lecture.* 30 July 1997

[7] R. Brun, N. Buncic, V. Fine and F. Rademakers. *ROOT, Overview.* Code-CERN (1996).

[8] W.H. Press, B.P. Flannery, S.A. Teukolsky and W.T Vetterling. *Numerical Recipes in C.* Cambridge University Press, Cambridge. (1989) (104-05,212-13).

[9] L. Lyons. *Statistics for Nuclear and Particle Physicists.* Cambridge University Press, Cambridge. (1986).

[10] D.C. Carey. *The Optics of Charged Particle Beams.* Hardwood Academic Publishers, Lhomond. (1987).